ceramics

MDPI

Article

Electron-Beam Sintering of Al_2O_3-Cr-Based Composites Using a Forevacuum Electron Source

Aleksandr Klimov [1,*], Ilya Bakeev [1], Anna Dolgova [1], Efim Oks [1,2], Van Tu Tran [1] and Aleksey Zenin [1]

[1] Laboratory of Plasma Electronics, Tomsk State University of Control Systems and Radioelectronics, 634050 Tomsk, Russia
[2] Laboratory of Plasma Sources, Institute of High Current Electronics SB RAS, 634034 Tomsk, Russia
* Correspondence: klimov@main.tusur.ru; Tel.: +7-905-990-5241

Abstract: We describe our studies of the influence of Cr content in an Al_2O_3-Cr composite on its thermal and electrical conductivity properties during and after electron-beam sintering in the forevacuum range of pressure. Sintering was carried out using a plasma-cathode forevacuum-pressure electron source of an original design, capable of processing non-conducting materials directly. It is shown that the chromium content affects the efficiency of the beam power transfer to the irradiated composite. The efficiency decreases with increasing chromium content. Measurement of the composite's coefficient of thermal conductivity, in the temperature range 50–400 °C, shows that it varies almost linearly from 25 W/(m·K) to 68 W/(m·K) as the Cr content in the composite increases from 25% to 75% wt. The electrical conductivity properties after sintering exhibit a non-linear behavior. The conduction activation energy E_a, measured via the dependence of the current through composites of different compositions, is slightly lower than the Al_2O_3 band-gap. The addition of metallic Cr results in a disproportionate decrease in E_a, almost by an order of magnitude, from 6.9 eV to 0.68 eV. By varying the chromium content, it is possible to form a material with thermal and electrical conductivities controllable over a wide range.

Keywords: pressureless sintering; composite ceramics; electron beam; electron-beam irradiation; sintering; conduction activation energy; Al_2O_3-Cr; thermal conductivity; electrical conductivity; forevacuum pressure region

Citation: Klimov, A.; Bakeev, I.; Dolgova, A.; Oks, E.; Tran, V.T.; Zenin, A. Electron-Beam Sintering of Al_2O_3-Cr-Based Composites Using a Forevacuum Electron Source. *Ceramics* **2022**, *5*, 748–760. https://doi.org/10.3390/ceramics5040054

Academic Editor: Amirhossein Pakseresht

Received: 12 September 2022
Accepted: 11 October 2022
Published: 14 October 2022

1. Introduction

Metal–ceramic composites offer numerous advantages. They are materials of high hardness and mechanical strength that can operate at temperatures above 1000 °C [1]. Wide commercial use of composites is possible, contingent upon the availability of rapid production methods and a good understanding of their thermal and electrical characteristics. Of the various kinds of ceramic materials, Al_2O_3-based ceramic is one of the most widely used, possessing high strength, high hardness, and excellent thermal resistance [2–5]. However, its high brittleness restricts its possible applications. The introduction of malleable metal phases to ceramics is an effective method of reducing its brittleness. Metal–ceramic composites obtained in this way acquire not only low brittleness but also often new electrical, optical, magnetic, and thermal properties [6–11]. In the work described here, for the metallic component we select Cr, which has a high melting point (1863 °C [12]), high-temperature oxidation resistance, and high-temperature plasticity [13,14]. These properties may be useful in creating thermally, chemically, and mechanically strong metal–ceramic materials. Among the main areas of application of such materials are the coating of jet nozzles and the protective coating of gas furnaces, crucibles, heat shields, etc.

The main methods used for forming composite materials can be divided into two types. The first is selective sintering by an electron or laser beam [15,16], and the second includes hot pressing, [17,18], cold pressing, microwave, thermal [19], and spark plasma

sintering [20–22]. The sintering of powders involves issues with controlling the heating rate and the uniformity of target heating. Furnace heating and sintering require time-consuming exposure at high temperatures and have low energy efficiency. When a target is irradiated by laser radiation, heating of the material starts from the surface and proceeds to the core unevenly [23]. This temperature gradient leads to uneven distribution of grain size and of density with depth [24]. These problems can be resolved by lowering the heating rate, thereby increasing the overall processing time. Additionally, the efficiency of the laser energy transfer to the target depends on its optical properties, which restricts the range of materials that can be used for sintering.

In the case of target heating by an electron beam, the target optical properties are not important. However, a new problem arises, which is removing the electrical charge carried by the electron beam onto the dielectric target. The charged surface causes electron beam defocusing and diminishes the efficiency of the beam power transfer to the irradiated target [25,26]. This issue can be resolved by use of a forevacuum-pressure plasma-cathode electron source for the e-beam irradiation. Such sources generate electron beams at a pressure of 1–100 Pa, and the negative surface charge is compensated by the positive ion flux from the beam plasma created during beam propagation at such elevated pressure values [27]. We have previously shown [28–30] that the use of electron beams generated by forevacuum plasma electron sources is a useful approach for sintering ceramic compacts. In the work described here, we have used this method for electron-beam sintering of Al_2O_3-Cr-based composites and have explored the thermal and electrical properties of the Al_2O_3-Cr composites produced.

2. Materials and Methods

We used commercially available Al_2O_3 powders with particle size 10–30 μm, and Cr powder with particle size 50 μm.

The main parameters pertaining to the experiment are shown in Table 1 [31–34].

Table 1. Material parameters at 20 °C.

Material	Theoretical Density, g/cm^3	Thermal Conductivity, W/(m·K)	Melting Point, °C	Specific Electrical Conductivity, S/m	Band Gap, eV
Al_2O_3	3.97	27–34	2054	10^{-9}–10^{-11}	5.1–8.7
Cr	7.19	93.9	1907	5.104×10^6	-

The composites for sintering were produced by mixing ceramic and metal powders in various mass proportions. The sample and the mixture used to produce it were assigned the same nomenclature label. The proportions are shown in Table 2.

Table 2. Mixture contents used to prepare Al_2O_3-Cr composite.

Mixture Label	Al_2O_3 Content, % wt.	Cr Content, % wt.
100A	100	0
75A	75	25
50A	50	50
25A	25	75

Pellets 3 ± 0.1 mm thick and 10 ± 0.1 mm in diameter were formed from the mixtures by uniaxial pressing. The composites were processed in a vacuum chamber equipped with necessary pumping equipment and manipulators; see Figure 1a. A forevacuum plasma-cathode electron source [35] was used for composite heating. A beam-focusing system of a special design allowed an electron beam of 0.6 mm in diameter to be generated in the vacuum chamber, under forevacuum conditions at a pressure of 30 Pa (helium). For

sintering, the composite of given composition was placed in the vacuum chamber on a graphite holder of special design. The holder assembly consisted of a graphite crucible with mounting and bracing that minimized heat loss to its fastening elements. The composite heating efficiency was improved by placing a heat-reflecting shield around the graphite holder to reduce heat transfer to the chamber walls by thermal radiation. After installing the composite and evacuating the chamber to a working pressure of 3.0 Pa, the electron source was turned on. Sintering was performed as follows. First, a smooth heating of the composite at constant electron beam energy of 15 keV, by slowly increasing the beam current from 10 to 100 mA, depending of the composite composition; then, exposure to the beam at a constant temperature of 1400 °C for 10 minutes; next, cooling by reducing the beam current, followed by turning off the electron source and further cooling in the vacuum chamber for 20 minutes. Since the area of the irradiated surface was much greater than the cross-sectional area of the electron beam at its point of incidence on the composite, the electron beam was rapidly scanned over the composite surface. The scanning was performed using a magnetic deflecting system controlled by a sweep circuit. The scanning frequency was 100 Hz, and the scanned area was 1 × 1 cm^2.

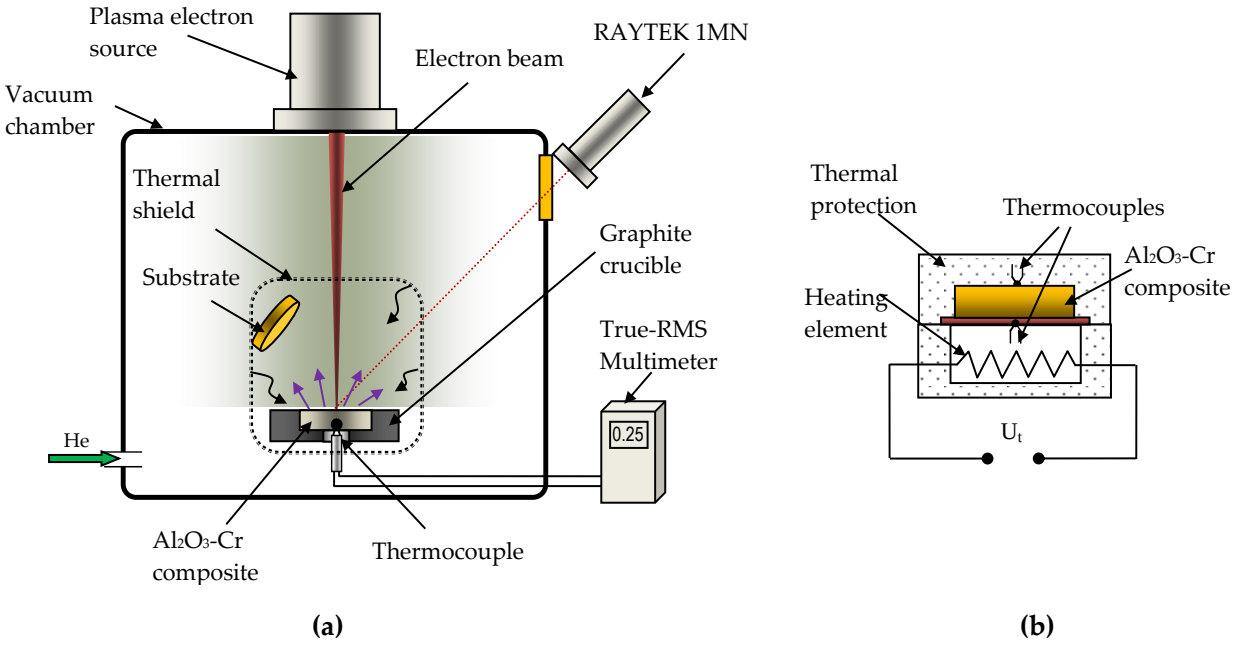

Figure 1. Schematic diagram of the experimental setup (**a**) and electrical heater (**b**).

The composite surface during sintering was monitored remotely by a RAYTEK 1MH (Raytek Corp., Santa Cruz, CA, USA) infrared pyrometer with measurement range 550–3000 °C. A tungsten–rhenium thermocouple was used to measure the temperature of the composite non-irradiated side. The thermocouple and the composite surface were in tight contact with each other. The thermocouple and the pyrometer were calibrated by heating of a thin copper plate. The difference in readings did not exceed 10 °C.

Current through the composite during its irradiation was measured by replacing the thermocouple with a flat metal electrode (not shown in Figure 1). The sample was placed on this electrode on the irradiated side. The current through the sample was measured by a True-RMS Multimeter 289 (Fluke Corp., Everett, WA, USA), with one sensing wire connected to the electrode and the other grounded.

In order to investigate the thermal properties of the composites after sintering, a model of an electrical heater was made; see Figure 1b. The heater could heat composite materials up to 400 °C in a controlled manner. In addition, it was possible to measure the heat flow through the samples and to measure the temperature of the irradiated and non-irradiated surfaces. The temperature was measured using standard chromel–copel thermocouples.

Sample microstructure and elemental composition were studied using a JEOL JSM-7500FA (JEOL Ltd., Freising, Germany) scanning electron microscope, equipped with a set of add-on units for energy dispersive elemental analysis (EDS) and electron backscatter diffraction (EBSD) (Bruker Nano GmbH, Berlin, Germany). We used the facilities at the TPU Center for Sharing Use, "Nanomaterials and Nanotechnologies", supported by the Ministry of Education and Science of Russia under grant number 075-15-2021-710.

3. Experimental Results and Analysis

3.1. Electron-Beam Sintering

Focused electron-beam heating in the forevacuum medium enabled us to heat the composite surfaces quite easily to temperatures of 800–900 °C. The temperature growth rate at constant beam power of 40 W/min was 80 °C/min; see Figure 2.

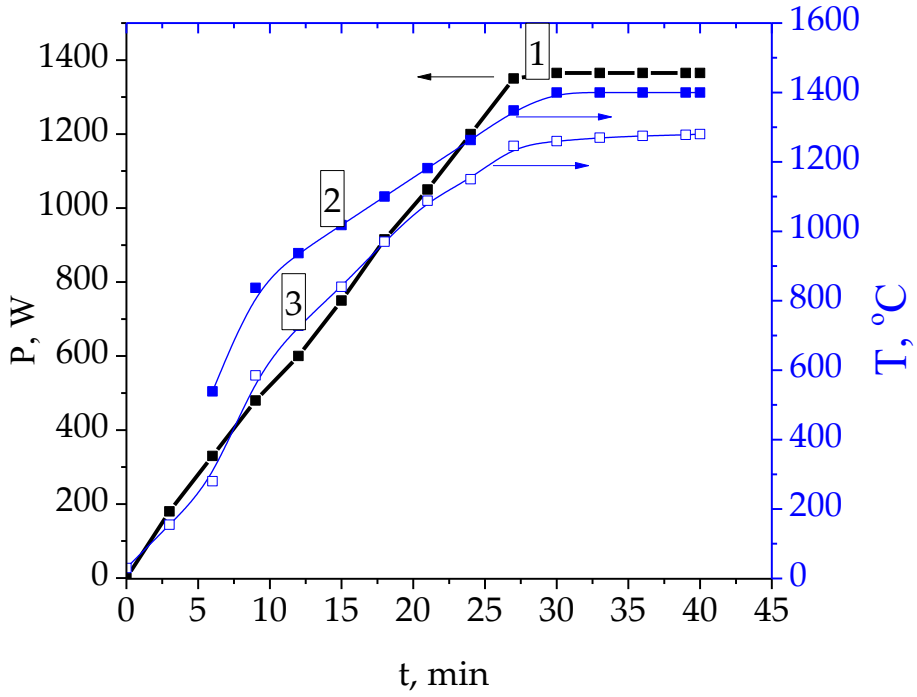

Figure 2. Dependencies of the electron beam power 1 and the temperature of irradiated 2 and non-irradiated 3 surfaces of the 75A composite, as a function of time.

The sample temperature growth rate decreased to 26–30 °C/min, depending on the chromium content in the composite. The temperature-increase rate for zero chromium content is 30 °C/min, and the addition of chromium decreases the temperature growth rate to 26 °C/min. This change in the rate of temperature rise is not significant, but is still noticeable. Clearly the thermal parameters, especially the coefficient of thermal conductivity, affect the composite heating. Since chromium has a greater coefficient of thermal conductivity than aluminum oxide, 94 W/(m·K) and, on average, 30 W/(m·K), respectively, the addition of chromium results in greater heat transfer to the graphite crucible and the holder elements, thereby reducing the composite heating. This circumstance should be taken into account when automating and optimizing the process.

3.2. Microstructure and Parameters

After sintering, the samples were cut in half along a diameter and were polished. In order to remove the products of grinding, they were then rinsed in alcohol and distilled water in an ultrasonic bath for 20 minutes. The microstructures of 75A, 50A, and 25A composites are shown in Figure 3. The samples display homogeneous areas with good compaction, as well as pores of various sizes formed at grain boundaries. EDX analysis

revealed that the gray areas correspond to Al_2O_3 ceramic matrix and the lighter areas are Cr. The size of Al_2O_3 grains is 20–40 µm, and the size of Cr grains is 20 to 80 µm. With the increase in Cr content, the Cr grain size increases due to smaller grains amalgamating into bigger grains.

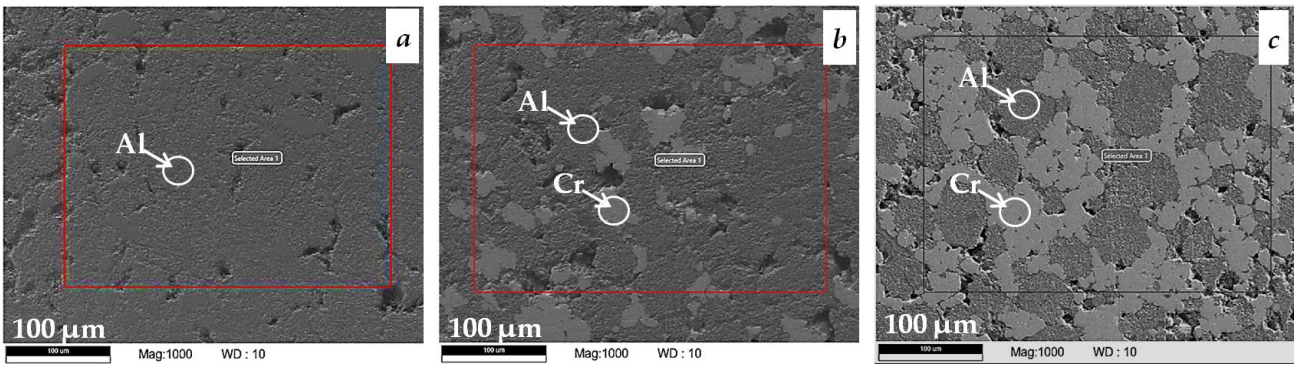

Figure 3. SEM image of composite microstructure for samples (**a**) 75A, (**b**) 50A, and (**c**) 25A.

The elemental composition of the selected areas, obtained by energy-dispersive analysis, is shown in Figure 4. The increase in Cr content corresponds to its content in the initial mixture of powders used for sintering.

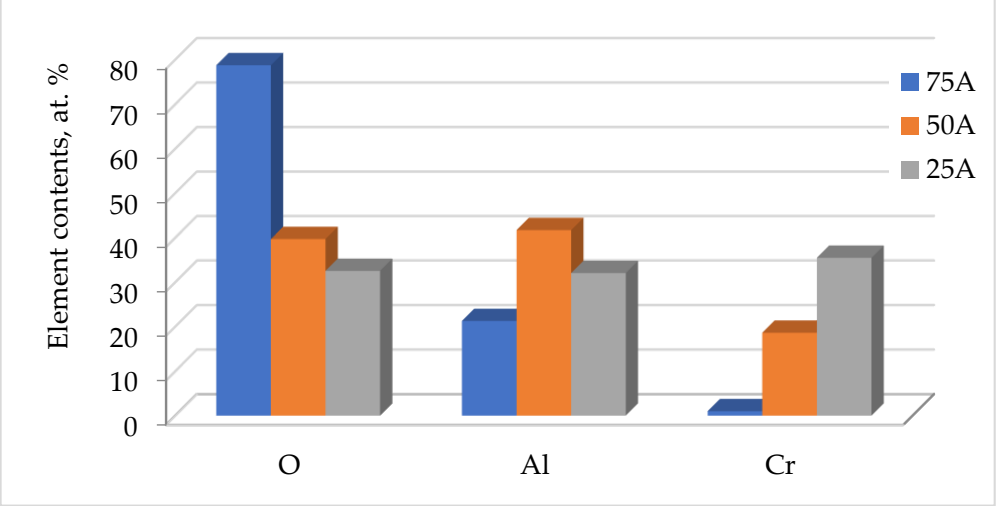

Figure 4. Contents of O, Al, and Cr in the cross sections of 75A, 50A, and 25A composites.

Composite parameters before and after electron-beam sintering are shown in Table 3.

Table 3. Composite parameters before and after sintering.

Sample		100A	75A	50A	25A
Mass m, mg	before	395	420	493	610
	after	356	401	479	580
Thickness h, mm	before	2.78	2.83	2.82	2.73
	after	2.6	2.63	2.68	2.61
Diameter d, mm	before	10.3	10.32	10.23	10.30
	after	9.32	9.54	9.69	9.86
Density ρ, g/cm^3	before	1.7	1.77	2.13	2.68
	after	2.02	2.14	2.43	2.92

The maximum increase in density after irradiation, 21%, was for the composite containing 75% aluminum oxide. The minimum increase in density, 9%, was for the 25A sample, with the lowest content of Al_2O_3. It is apparent that since aluminum oxide has greater shrinkage in the course of sintering, the corresponding samples with greater content of it must have smaller geometric dimensions and, hence, a higher density after sintering. Compared with the sintering of similar composites using the hot-pressing method [36], the porosity value in this work turned out to be higher. This difference may be due to the peculiarity of the electron beam method—sintering without applying pressure.

The mass of all composites changes (decreases) after sintering; see Table 3. A possible reason could be mass evaporation during sintering. However, the sintering temperature of 1400 °C is not high enough for melting and evaporating the composite components; see Table 1. To further explore the possibility of mass loss by evaporation, we conducted experiments to study the composition of coatings on witness substrates. Substrates in the form of flat steel disks were placed at a distance of 5 cm from the sintered composite, as shown in Figure 1. After sintering, the sample surface elemental composition was studied by energy-dispersive analysis. According to the composition measurements for three compacts, the substrate coatings contained elemental constituents of the composites, namely chromium and aluminum; see Figure 5.

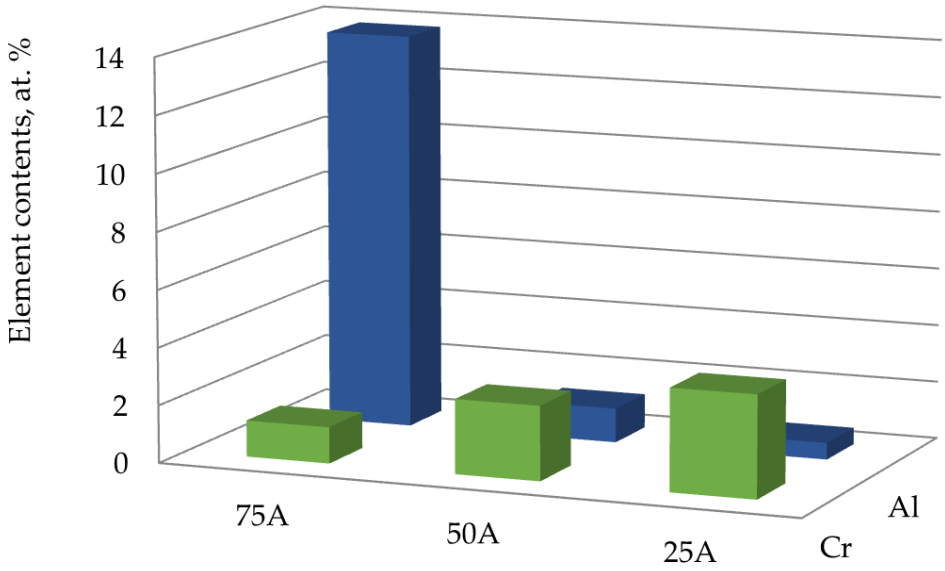

Figure 5. Contents of Al and Cr in the witness substrate coatings: 75A, 50A, and 25A.

As shown in Figure 5, the coatings contain a significant amount of the composite elements. Thus, for the composite with 75% aluminum oxide (75A), the substrate coating contains over 13% at. aluminum. The witness substrates used for the other composites with a lower aluminum oxide content demonstrate a considerable decrease in aluminum in the coating. For the 50A composite, the aluminum content on the substrate is less than for 75A, by almost a factor of 10. At the same time, the chromium content in the substrate coating increases almost proportionally to the increase in chromium content in the sintered composite—from 1.26% for composite 75A with 25% Cr to 3.56% for composite 25A with 75% Cr. Evidently, these elements appear on the substrate due to evaporation from the composite surface. Despite the rather low temperature, according to pyrometer readings, for the evaporation of these elements to occur, such an effect can occur during electron-beam sintering of ceramics employing an electron beam deflecting system. When scanning the ceramic surface, the high power-density electron beam can cause local heating of the surface at the impact point; the beam cross-section at the impact point is less than 1 mm^2. Since the pyrometer measures the mean value of the composite surface temperature over an area of about 2.5 cm^2, the local temperature increase at the beam impact point is not

readily registered. Additionally, mass loss from the composite surface can occur due to evaporation of low-melting-point impurities with a content in the aluminum oxide powder used in the experiments that can be as high as 5%.

Another possible mechanism for heating to the evaporation temperatures of Al_2O_3 and Cr could be heating due to the current through the composite bulk, as is the case for the flash-sintering technique. In this technique, a constant electric field of 100–150 V/m is established between the two opposite surfaces of the sintered sample, which is simultaneously heated to a high temperature. The electrical conduction, arising as a result of the temperature increase, leads to Joule heating of the sample. This significantly reduces the ceramic sintering time.

Measurement of the current through the composite show that it can reach several milliamperes; see Figure 6.

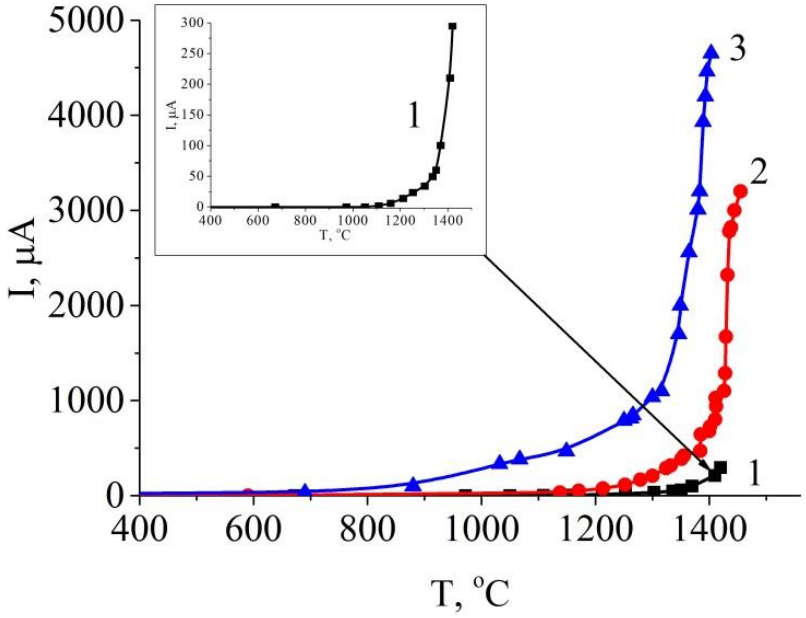

Figure 6. Temperature dependence of current through composites during electron-beam sintering: (1) composite 75A; (2) composite 50A; (3) composite 25A.

The current increases with increasing chromium content, which is directly related to the increase in the composite electrical conductivity. The addition of a metal, as a more electrically conducting material, increases the overall electrical conductivity of the composite. The dependence of the coefficient of electrical conductivity is well-known to be exponential with temperature:

$$\gamma = \gamma_0 \cdot \exp\left(-\frac{\Delta E_a}{kT}\right) \quad (1)$$

where

γ_0 is an electrical conductivity of the conductor/dielectric, S/m;

γ_0 is a temperature-independent coefficient determined by the properties of the conductor/dielectric, S/m;

k is Boltzmann's constant, J/K;

T is the temperature of the irradiated composite surface, K; and

E_a is the conduction activation energy, eV.

The conduction current in semiconductors, of which aluminum oxide may be referred to as a particular kind, depends on the coefficient of electrical conductivity, as well as on the field strength in the semiconductor. Assuming that the field strength is determined by the difference of potentials between the irradiated and non-irradiated surfaces, one can

write an equation for evaluating the value of the conduction current flowing through the composite as a function of temperature during electron-beam irradiation:

$$I_\gamma = \frac{\Delta\varphi}{h} \cdot S \cdot \gamma_0 \cdot \exp\left(-\frac{E_a}{kT}\right) \quad (2)$$

where

S is the composite base area, m^2;

$\Delta\varphi$ is the difference of potentials between the irradiated and non-irradiates surfaces of the composite, V; and

h is the composite thickness.

Expression (2) allows the conduction activation energy to be estimated for composites with different elemental contents. Assuming that the temperature dependence of the potential of the composite surface is not as strong as that of the coefficient of electrical conductivity and plotting the graphs $\ln(I) = f\left(\frac{1}{T}\right)$ using the experimental data of Figure 4, one can determine the activation energy from the slope of the straight lines obtained. The dependencies $\ln(I) = f\left(\frac{1}{T}\right)$, plotted for the three composites over the temperature range 1000–1400 °C, where a noticeable increase in current is observed, are shown in Figure 7. As can be seen, the experimental points of the logarithm of the current from the inverse temperature fit into a linear dependence. From one perspective, this serves as an argument in favor of the chosen mechanism for increasing electrical conductivity with increasing temperature and the correctness of choosing Formula (1) for theoretical estimates.

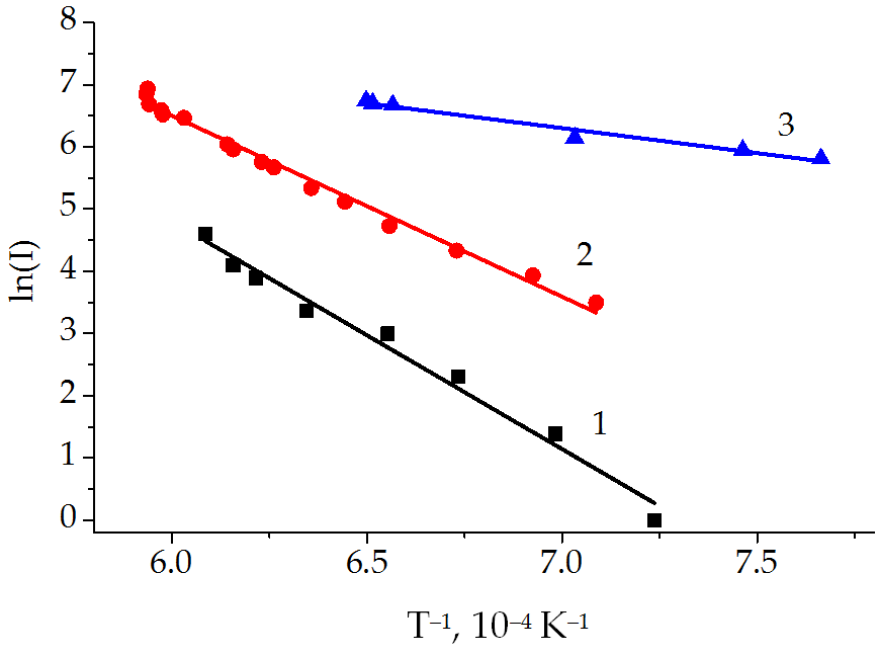

Figure 7. Temperature dependencies $\ln(I) = f\left(\frac{1}{T}\right)$ for composites of different compositions: (1) composite 75A; (2) composite 50A; (3) composite 25A.

The fact that the experimental data fit well to straight lines indirectly indicates that the assumption not to take into account the change in potential on the composite surface over the given temperature range is correct.

The calculated values of the conduction activation energy E_a are given in Table 4.

Table 4. Conduction activation energy for composites of different compositions.

Sample	75A	50A	25A
E_a, eV	3.1 ± 0.4	2.5 ± 0.3	0.68 ± 0.08

The obtained values of E_a for the Cr-containing composites are slightly lower than the Al_2O_3 band gap, which is predictable, since it was a metal that was added to the composite. The addition of metallic Cr results in a disproportional decrease in E_a. Thus, for the composite with 25% chromium content, the conduction activation energy, or band gap, decreases compared to pure Al_2O_3, from an average value of 6.9 eV (see Table 2) to 3.1 eV, i.e., by more than a factor of two. The addition of 75% Cr leads to a further decrease in E_a, down to 0.68 eV, which is almost by an order of magnitude.

As shown in [37], the electrical conductivity of aluminum oxide-based composites can be adjusted, when reinforced with conductive or semi-conductive phases (such as silicon carbide, for example), added in an amount at which they penetrate into an insulating aluminum oxide matrix. After sintering, such a composite can be used in many industries. The main factors affecting the electrical properties of composites with reinforced semiconductor phases are the volume fraction of SiC and the content of other impurities. The addition of SiC improves the electrical conductivity, which increases with an increase in the volume fraction of SiC [37]. Thus, in a composite with 20 vol.% SiC, the conductivity of 4.05×10^{-2} S·m^{-1} was measured, which is an increase of four orders of magnitude compared to the reference monolithic alumina (7.80×10^{-6} S·m^{-1}).

A rather strong dependence of the composite electrical conductivity on the content of metal phase has been observed [38], when adding Ti to an Al_2O_3 ceramic matrix. Specific electrical resistance, with the addition of 20% vol. Ti, decreases from 10^{12} Ohm·m to 10^{-2}–10^{-3} Ohm·m, and the fall is rather abrupt. The authors have explained this by the formation of conducting paths through the composite bulk, due to the melting of fine grains of Ti. In the present work, the changes are not so severe, which may be related to pressureless sintering. Chromium grains combine without forming conducting paths throughout the composite volume; see Figure 3.

The electrical parameters of the Al_2O_3-Cr composite can be controlled over a fairly wide range.

3.3. Composite Thermal Conductivity

Thermal conductivity is an important parameter in such applications of Al_2O_3 ceramics as high-temperature structural components, refractories, gas burners, wear parts, and cutting tools. To reduce thermal shock, the thermal conductivity of the composite in all these applications should be as high as possible. It can be expected that Cr particles improve the thermal conductivity of Al_2O_3-based composites due to the inherent high thermal conductivity of Cr.

To measure the thermal conductivity, the sintered composites were placed in a heating device with a fixed heater temperature T_1 and a temperature T_2 on the composite side not subject to irradiation; see Figure 1b. The coefficient of thermal conductivity λ was determined using the expression:

$$\lambda = \frac{Q \cdot h}{\Delta T \cdot S} \quad (3)$$

where λ is the coefficient of thermal conductivity, W/(m·K);

Q is the heat flux through the composite, W/m^2;

ΔT is the difference of temperatures: $T_1 - T_2$, °C; and

S is the composite surface area, m^2.

The obtained value of the coefficient of thermal conductivity corresponds to the average temperature $\Delta T/2$.

The measured thermal conductivity over the temperature range 50–400 °C is shown in Figure 8. As seen, the coefficient of thermal conductivity decreases with increasing

temperature for composites of any composition, as reported in the literature [39]. The general pattern here is as follows: the thermal conductivity of ceramics of a crystalline structure, especially an oxide, with an increase in temperature, as a rule, drops significantly [40]. This is based on the idea of heat transfer in solid non-metallic bodies by thermal elastic waves—phonons. The thermal conductivity of the composite is closely related to their microstructure and depends on the free path length of the phonons: the degree of disturbance of the harmonic oscillations of heat waves during their passage through a given substance. Phonons are also known to interact with lattice defects, grain boundaries, and other microstructure defects. The presence of a metallic phase in the form of chromium inclusions leads to a higher porosity value, characteristic of composites and, as a result, negatively affect thermal conductivity. The resulting internal stresses in composites also lead to a decrease in thermal conductivity [41]. However, despite these negative factors, the thermal conductivity of the composite increases with an increase in the chromium content and is still higher than that of pure aluminum oxide.

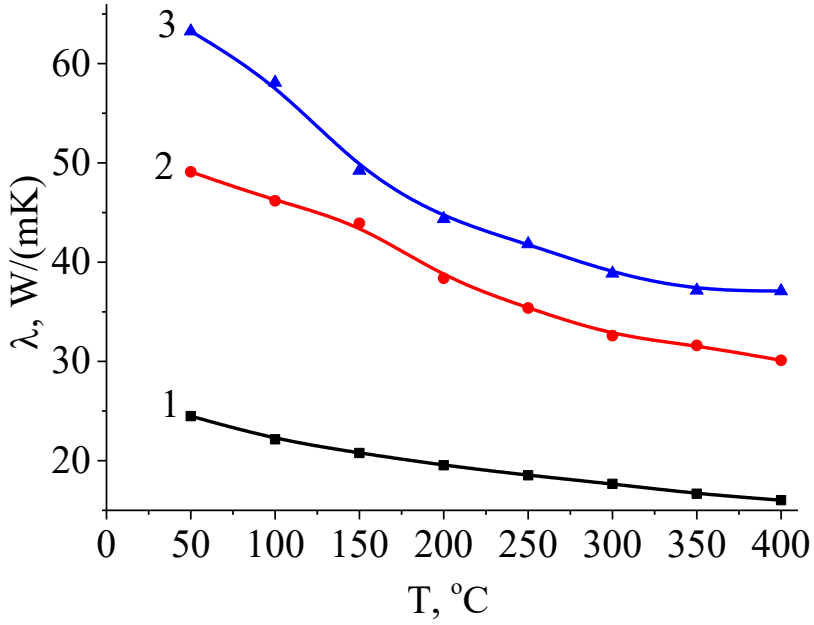

Figure 8. Temperature dependence of thermal conductivity for composites of different compositions: (1) composite 75A; (2) composite 50A; (3) composite 25A.

The coefficient of thermal conductivity of the composite with 75% content of Al_2O_3 is 25 W/m·K and does not differ significantly from that of pure Al_2O_3 at the same temperature [42]. The values of thermal conductivity measured at room temperature are somewhat lower than the data given in the literature [43] and are measured for mono-cast Al_2O_3 (28–30 W/m·K). A possible reason is the greater porosity of the materials obtained in this work. With the addition of Cr, the composite conductivity rises almost proportionally to the content of Cr. Thus, for the composite with 75% content of Cr, i.e., three times as much compared to that in the 25% Cr composite, the conductivity increases from 25 to 68 W/m·K. For both Al_2O_3 and Cr, the thermal conductivity decreases with temperature [44], as is reflected in Figure 8. Compared with the data of [45], the thermal conductivity of the composite remains at a high level and does not decrease to values below 15 W/m·K.

4. Conclusions

Electron-beam irradiation allows Al_2O_3-Cr-based composites to be sintered at a temperature of 1400 °C. The complete sintering cycle, including heating and cooling, is no longer than 50 minutes. By varying the Cr content, one can change the electrical and thermal conductivity properties of the composite. In this case, the thermal conductivity in

the temperature range of 20–400 °C varies directly proportionally to the Cr content and inversely proportionally to temperature. The thermal conductivity increases from 25 to 68 W/m·K, when the Cr content increases from 25% to 75%, and decreases with increasing temperature, especially for composites with higher Al_2O_3 content.

The electrical conductivity properties, illustrated by the current through the composite and the conduction activation energy, depend on the Cr content nonlinearly. The addition of 75% Cr to the composite decreases the Al_2O_3-Cr activation by an order of magnitude compared to that of Al_2O_3, from 6.9 to 0.68 eV. At the same time, the addition of 50% Cr reduces this energy only by a factor of two, to 2.5 eV. In general, by varying the chromium content, it is possible to produce materials with values of electrical conductivity controllable over orders of magnitude and thermal conductivity controllable within range limits differing by almost a factor of two.

Author Contributions: Conceptualization, A.K. and E.O.; methodology, A.Z.; software, A.D.; validation, A.K., A.Z., and I.B.; formal analysis, A.K.; investigation, A.Z. and V.T.T.; resources, E.O.; data curation, A.K.; writing—original draft preparation, A.K.; writing—review and editing, E.O.; visualization, I.B.; supervision, E.O.; project administration, A.K.; funding acquisition, A.K. and V.T.T. All authors have read and agreed to the published version of the manuscript.

Funding: The work was supported by grant FEWM-2020-0038 from the Ministry of Science and Higher Education of the Russian Federation, and a study of coatings composition was funded by research project 20-38-90184 from RFBR.

Institutional Review Board Statement: Not applicable.

Informed Consent Statement: Not applicable.

Data Availability Statement: Not applicable.

Acknowledgments: Special thanks to Ian Brown (Berkeley Lab) for the English correction and helpful discussion.

Conflicts of Interest: The authors declare no conflict of interest. The funders had no role in the design of the study; in the collection, analyses, or interpretation of data; in the writing of the manuscript; or in the decision to publish the results.

References

1. Foltz, J.V.; Blackmon, C.M. *Metal Matrix Composites in Metals Handbook*, 10th ed.; Second Print, Properties and Selection; ASM: Metals Park, OH, USA, 1992; Volume 2, p. 2536.
2. Fan, R.; Liu, B.; Zhang, J.; Bi, J.; Yin, Y. Kinetic evaluation of combustion synthesis $3TiO_2 + 7Al \rightarrow 3TiAl + 2Al_2O_3$ using non-isothermal DSC method Mater. *Chem. Phys.* **2005**, *91*, 140–145.
3. Niu, F.Y.; Wu, D.J.; Zhou, S.Y.; Ma, G.Y. Power prediction for laser engineered net shaping of Al_2O_3 ceramic parts. *J. Eur. Ceram. Soc.* **2014**, *34*, 3811–3817. [CrossRef]
4. Reddy, M.P.; Ubaid, F.; Shakoor, R.A.; Parande, G. Effect of reinforcement concentration on the properties of hot extruded Al-Al_2O_3 composites synthesized through microwave sintering process. *Mater. Sci. Eng. A* **2017**, *696*, 60–69. [CrossRef]
5. Ramesh, M.; Marimuthu, K.; Karuppuswamy, P.; Rajeshkumar, L. Microstructure and properties of YSZ-Al_2O_3 functional ceramic thermal barrier coatings for military applications. *Bol. Soc. Esp. Cerám. Vidr.* 2021, *in press*. [CrossRef]
6. Pietrzak, K.; Chmielewski, M.; Wlosinski, W. Sintering Al_2O_3–Cr composites made from micro-and nanopowders. *Sci. Sinter.* **2004**, *36*, 171–177. [CrossRef]
7. Oh, S.T.; Sekino, T.; Niihara, K. Fabrication and mechanical properties of 5 vol% copper dispersed alumina nanocomposites. *J. Eur. Ceram. Soc.* **1998**, *18*, 31–37. [CrossRef]
8. Sekino, T.; Nakahira, A.; Nawa, M.; Niihara, K. Fabrication of Al2O3/W nanocomposites. *J. Powder Metal.* **1991**, *38*, 326–330. [CrossRef]
9. Pan, Y.; Xiao, S.; Lu, X.; Zhou, C.; Li, Y.; Liu, Z.; Qu, X. Fabrication, mechanical properties and electrical conductivity of Al_2O_3 reinforced Cu/CNTs composites. *J. Alloys Compd.* **2019**, *782*, 1015–1023. [CrossRef]
10. Hossain, S.; Rahman, M.M.; Chawla, D.; Kumar, A.; Seth, P.P.; Gupta, P.; Jamwal, A. Fabrication, microstructural and mechanical behavior of Al-Al_2O_3-SiC hybrid metal matrix composites. *Mater. Today Proc.* **2020**, *21*, 1458–1461. [CrossRef]
11. Farvizi, M.; Javan, M.K.; Akbarpour, M.R.; Kim, H.S. Fabrication of NiTi and NiTi-nano Al_2O_3 composites by powder metallurgy methods: Comparison of hot isostatic pressing and spark plasma sintering techniques. *Ceram. Int.* **2018**, *44*, 15981–15988. [CrossRef]
12. Okamoto, H. The Cr-O (chromium-oxygen) system. *J. Phase Equilb.* **1997**, *18*, 402. [CrossRef]

13. Gulbransen, E.A.; Andrew, K.F. Kinetics of the oxidation of chromium. *J. Electrochem. Soc.* **1957**, *104*, 334–338. [CrossRef]
14. Holzwarth, U.; Stamm, H. Mechanical and thermomechanical properties of commercially pure chromium and chromium alloys. *J. Nucl. Mater.* **2002**, *300*, 161–177. [CrossRef]
15. Pfeiffer, S.; Florio, K.; Puccio, D.; Grasso, M.; Colosimo, B.M.; Aneziris, C.G.; Graule, T. Direct laser additive manufacturing of high performance oxide ceramics: A state-of-the-art review. *J. Eur. Ceram. Soc.* **2021**, *41*, 6087–6114. [CrossRef]
16. Vailes, J.; Hagedorn, Y.C.; Wilhelm, M.; Konrad, W. Additive manufacturing of ZrO_2-Al_2O_3 ceramic components by selective laser melting. *Rapid Prototyp. J.* **2013**, *19*, 51–57.
17. Nguyen, T.D.; Caccia, M.; McCormack, C.K.; Itskos, G.; Kenneth, H.S. Corrosion of Al_2O_3/Cr and Ti_2O_3/Cr composites in flowing air and CO_2 at 750 °C. *Corros. Sci.* **2021**, *179*, 109115. [CrossRef]
18. Zhang, X.; Zhang, Y.; Tian, B.; Jia, Y.; Liu, Y.; Song, K.; Volinsky, A.A.; Xue, H. Cr effects on the electrical contact properties of the Al_2O_3-Cu/15W composites. *Nanotechnol. Rev.* **2019**, *8*, 128–135. [CrossRef]
19. Betül, K.Y.; Hüseyin, Y.; Yahya, K.T. Evaluation of mechanical properties of Al_2O_3–Cr_2O_3 ceramic system prepared in different Cr_2O_3 ratios for ceramic armour components. *Ceram. Int.* **2019**, *45*, 20575–20582.
20. Pulgarín, H.L.C.; Albano, M.P. Sintering and Microstructure of Al_2O_3 and Al_2O_3-ZrO_2. *Ceramics. Procedia Mater. Sci.* **2015**, *8*, 180–189. [CrossRef]
21. Daguano, J.K.M.F.; Santos, C.; Souza, R.C.; Balestra, R.M.; Strecker, K.; Elias, C.N. Properties of ZrO_2–Al_2O_3 composite as a function of isothermal holding time. *Int. J. Refract. Met. Hard Mater.* **2007**, *25*, 374–379. [CrossRef]
22. Maca, K.; Pouchly, V.; Shen, Z. Two-step sintering and spark plasma sintering of Al_2O_3, ZrO_2 and $SrTiO_3$ ceramics. *Integr. Ferroelectr.* **2008**, *99*, 114–124. [CrossRef]
23. Liu, X.; Zou, B.; Xing, H.; Huang, C. The preparation of ZrO2-Al2O3 composite ceramic by SLA-3D printing and sintering processing. *Ceram. Int.* **2019**, *46*, 937–944. [CrossRef]
24. Hu, K.; Li, X.; Qu, S.; Li, Y. Effect of Heating Rate on Densification and Grain Growth During Spark Plasma Sintering of 93W-5.6Ni-1.4Fe Heavy Alloys. *Metall. Mater. Trans.* **2013**, *44*, 4323–4336. [CrossRef]
25. Luo, G.N.; Yamaguchi, K.; Terai, T.; Yamawaki, M. Charging effect on work function measurements of lithium ceramics under irradiation. *J. Alloys Compd.* **2003**, *349*, 211–216. [CrossRef]
26. Mekni, O.; Goeuriot, D.; Damamme, G.; Raouadi, K.; Sao, S.J.; Meunier, C.; Aoufi, A. Dynamic investigation of charging kinetics in sintered yttria stabilized zirconia and α-alumina polycrystalline ceramics under electron beam irradiation. *Ceram. Int.* **2016**, *42*, 8729–8737. [CrossRef]
27. Burdovitsin, V.A.; Klimov, A.S.; Medovnik, A.V.; Oks, E.M. Electron beam treatment of non-conducting materials by a fore-pump-pressure plasma-cathode electron beam source. *Plasma Sources Sci. Technol.* **2010**, *19*, 055003. [CrossRef]
28. Klimov, A.S.; Bakeev, I.Y.; Dvilis, E.S.; Oks, E.M.; Zenin, A.A. Electron beam sintering of ceramics for additive manufacturing. *Vacuum* **2019**, *169*, 108933. [CrossRef]
29. Klimov, A.S.; Bakeev, I.Y.; Oks, E.M.; Zenin, A.A. Electron-beam sintering of an Al_2O_3/Ti composite using a forevacuum plasma-cathode electron source. *Ceram. Int.* **2020**, *46*, 22276–22281. [CrossRef]
30. Klimov, A.S.; Zenin, A.A.; Bakeev, I.Y.; Oks, E.M. Formation of gradient metalloceramic materials using electron-beam irradiation in the forevacuum. *Russ. Phys. J.* **2019**, *62*, 1123–1129. [CrossRef]
31. Abyzov, A.M. Aluminum oxide and alumina ceramics (Review). Part 1. Properties of Al_2O_3 and industrial production of dispersed Al_2O_3. *Novye Ogneup.* **2019**, *1*, 16–23. [CrossRef]
32. Jacobs, J.A.; Testa, S.M. Overview of Chromium (VI) in the Environment: Background and History. In *Chromium (VI) Handbook*, 1st ed.; CRC Press: Boca Raton, FL, USA, 2005; pp. 1–21.
33. Martienssen, W.; Warlimont, H. *Springer Handbook of Condensed Matter and Materials*; Springer: Berlin/Heidelberg, Germany, 2005; pp. 431–476.
34. Toyoda, S.; Shinohara, T.; Kumigashira, H.; Oshima, M.; Kato, Y. Significant increase in conduction band discontinuity due to solid phase epitaxy of Al_2O_3 gate insulator films on GaN semiconductor. *Appl. Phys. Lett.* **2012**, *101*, 231607. [CrossRef]
35. Klimov, A.; Bakeev, I.; Oks, E.; Zenin, A. Forevacuum plasma source of continuous electron beam. *Laser Part. Beams* **2019**, *37*, 203–208. [CrossRef]
36. Chmielewski, M.; Pietrzak, K. Processing, microstructure and mechanical properties of Al2O3–Cr nanocomposites. *J. Eur. Ceram. Soc.* **2007**, *27*, 1273–1279. [CrossRef]
37. Galusek, D.; Galusková, D. Alumina matrix composites with non-oxide nanoparticle addition and enhanced functionalities. *Nanomaterials* **2015**, *5*, 115–143. [CrossRef] [PubMed]
38. Shi, S.; Cho, S.; Goto, T.; Sekino, T. The effects of sintering temperature on mechanical and electrical properties of Al_2O_3/Ti composites. *Mater. Today Commun.* **2020**, *25*, 101522. [CrossRef]
39. Grimvall, G. *Thermophysical Properties of Materials*, 2nd ed.; Elsevier Science: Amsterdam, The Netherlands, 1999.
40. Parchovianský, M.; Galusek, D.; Švančárek, P.; Sedláček, J.; Šajgalík, P. Thermal behavior, electrical conductivity and microstructure of hot pressed Al2O3/SiC nanocomposites. *Ceram. Int.* **2014**, *14*, 14421–14429. [CrossRef]
41. Hasselman, D.P.H.; Johnson, L.F. Effective thermal conductivity of composites with interfacial thermal barrier resistance. *J. Compos. Mater.* **1987**, *21*, 508–515. [CrossRef]
42. Hostaša, J.; Pabst, W.; Matějíček, J. Thermal conductivity of Al_2O_3–ZrO_2 composite ceramics. *J. Am. Ceram. Soc.* **2011**, *94*, 4404–4409. [CrossRef]

43. McCluskey, P.H.; Williams, R.K.; Graves, R.S.; Tiegs, T.N. Thermal Diffusivity/Conductivity of Alumina—Silicon Carbide Composites. *J. Am. Ceram. Soc.* **1990**, *73*, 461–464. [CrossRef]
44. Moore, J.P.; Williams, R.K.; Graves, R.S. Thermal conductivity, electrical resistivity, and Seebeck coefficient of high-purity chromium from 280 to 1000 K. *J. Appl. Phys.* **1977**, *48*, 610–617. [CrossRef]
45. Wada, S.; Piempermpoon, B.; Nakorn, P.N.; Wasanapiarnpong, T.; Jinawath, S. Thermal conductivity of Al_2O_3 ceramics: The inconsistency between measured value and calculated value based on analytical models for a composite. *J. Sci. Res. Chula. Univ.* **2005**, *30*, 109–120.